Use of Wavelet Transforms in Analysis of Time–Activity Data from Cardiac PET

Jou-Wei Lin, Andrew F. Laine, Olakunle Akinboboye, and Steven R. Bergmann

Division of Cardiology, Department of Medicine, and Department of Radiology, College of Physicians and Surgeons, Columbia University, New York; and Department of Biomedical Engineering, Columbia University, New York, New York

Because of its intrinsic quantitative properties, PET permits measurement of myocardial perfusion and metabolism in absolute terms (i.e., mL/g/min). However, quantification has been limited by errors produced in image acquisition, selection of regions of interest, and data analysis. The goal of this study was to evaluate a newly developed, novel, wavelet-based noise-reduction approach that can objectively extract biologic signals hidden within dynamic PET data. **Methods:** Quantification of myocardial perfusion using dynamic PET imaging with ^{82}Rb, $H_2{}^{15}O$, and $^{13}NH_3$ was selected to evaluate the effects of the wavelet-based noise-reduction protocol. Dynamic PET data were fitted to appropriate mathematic models before and after wavelet-based noise reduction to get flow estimates. Time–activity curves, precision, accuracy, and differentiating capacity derived from the wavelet protocol were compared with those obtained from unmodified data processing. A total of 84 human studies was analyzed, including 43 at rest (18 ^{82}Rb scans, 18 $H_2{}^{15}O$ scans, and 7 $^{13}NH_3$ scans) and 41 after coronary hyperemia with dipyridamole (17 ^{82}Rb scans, 17 $H_2{}^{15}O$ scans, and 7 $^{13}NH_3$ scans). **Results:** For every tracer tested under all conditions, the wavelet method improved the shape of blood and tissue time–activity curves, increased estimate-to-error ratios, and maintained fidelity of flow in regions as small as 0.85 cm^3. It also improved the accuracy of flow estimates derived from ^{82}Rb to the level of that achieved with $H_2{}^{15}O$, which was not affected markedly by the wavelet process. In studies of patients with coronary disease, regional heterogeneity of myocardial perfusion was preserved and flow estimates in infarcted regions were differentiated more easily from normal regions. **Conclusion:** The wavelet-based noise-reduction method effectively and objectively extracted tracer time–activity curves from data with low signal-to-noise ratios and improved the accuracy and precision of measurements with all tracer techniques studied. The approach should be generalizable to other image modalities such as functional MRI and CT and, therefore, improve the ability to quantify dynamic physiologic processes.

Key Words: quantitative PET; myocardial blood flow; noise reduction; data analysis

J Nucl Med 2001; 42:194–200

Received Apr. 17, 2000; revision accepted Sep. 14, 2000.

For correspondence or reprints contact: Steven R. Bergmann, MD, PhD, Division of Cardiology, College of Physicians and Surgeons, Columbia University, PH 10-405, 630 W. 168th St., New York, NY 10032.

Cardiac PET is widely used clinically for the detection of coronary artery disease and for the assessment of myocardial viability. In addition, it provides a noninvasive approach to quantify myocardial perfusion and metabolism in absolute terms. However, PET-based quantification requires intensive computation of dynamic time–activity curves. Frequently, images have low signal-to-noise ratios, thus providing unreliable estimates of physiologic function.

Although PET images with $^{13}NH_3$ and $H_2{}^{15}O$ can measure myocardial perfusion accurately (*1–4*), dynamic curves are noisy at times and regional heterogeneity is high even in the hearts of healthy volunteers. This is contradictory to the fact that myocardial perfusion in the healthy subjects should be relatively homogeneous. In addition, accurate quantification using data from some tracers (e.g., ^{82}Rb) (*5,6*) has been difficult to achieve because of curves with low signal-to-noise ratios. There is intense interest in using ^{82}Rb because it is a generator-produced PET flow tracer and can be used at sites that do not have cyclotrons. Therefore, although quantification with dynamic PET can provide information in absolute terms, improvement in the fidelity of the underlying signal is still an important objective.

Several efforts have been made to reduce errors produced during image processing and data analysis (*7–10*). One approach is to apply kernels (mean filters, Gaussian filters, and so forth) or Fourier frequency filters to raw PET images or dynamic curves that are obtained from region-of-interest (ROI) analysis. It is also feasible to design a nonstationary filter to accommodate local changes and to create low-noise, high-contrast images (*11*). In spite of these efforts, image-based quantification is not always satisfactory and is, by nature, arbitrary and empiric.

We hypothesized that wavelet transforms and wavelet-based noise reduction ("denoising") could be used to improve image-based physiologic quantification with PET. The wavelet transform expands signals on the basis of compact (well localized) functions (wavelets). Because wavelets may have their energies concentrated in time or space, the wavelet transform, compared with the Fourier transform that represents a signal purely in the frequency domain, can simultaneously localize time (or space) and frequency components. Therefore, multiscale wavelet trans-

forms are especially well suited for the analysis of nonstationary signals, such as medical images and time–activity curves (*12*).

The wavelet coefficient thresholding and shrinkage method developed by Donoho and Johnstone (*13–15*) and adapted by Lin et al. (*16*) has several advantages over conventional smoothing methods. This algorithm transforms a noise-imposed signal into the wavelet domain, determines the local statistics of wavelet coefficients, finds a threshold value in the finest level of resolution, shrinks the amplitude of the coefficients by the threshold, and resynthesizes the signal. Wavelet denoising ensures that the reconstructed signal is at least as smooth as the underlying true function. Because of the built-in capacity of local adaptivity, this approach preserves the rapid rises and falls of a signal that are usually unintentionally and unavoidably smoothed by other existing methods. Most important, wavelet denoising has a solid mathematic background to support a near-optimal separation of signal and noise. This ability is objective and mathematically verifiable, whereas improvement with conventional filters is usually determined visually and empirically.

The aim of this study was to evaluate the effects of applying wavelet-based noise reduction on improving the fidelity of image-based physiologic quantification. Quantification of myocardial perfusion using dynamic PET images with ^{82}Rb, $H_2{}^{15}O$, and $^{13}NH_3$ was chosen for this study because of the importance of flow estimation, the rapid dynamic attributes of images, and the noise inherent in the curves.

MATERIALS AND METHODS

Subjects

The institutional review board of the Columbia-Presbyterian Medical Center approved this study. All subjects signed written informed consents. All studies were collected on an ECAT EXACT-47 whole-body PET scanner (CTI/Siemens, Knoxville, TN). Eighteen healthy volunteers with a low probability of coronary diseases were recruited. Dynamic PET scans using ^{82}Rb and $H_2{}^{15}O$ at rest and after pharmacologic stress with dipyridamole were obtained on 11 healthy subjects. For these scans, flow was estimated under resting conditions with ^{82}Rb followed by $H_2{}^{15}O$. Forty-five minutes after dipyridamole, the sequence was repeated. Seven subjects repeated the same protocol a few months later. Seven other healthy volunteers underwent dynamic scanning with $^{13}NH_3$ at rest and after dipyridamole. Thirteen patients with documented coronary disease were also enrolled. Each patient had PET scans with ^{82}Rb and ^{18}F-FDG at rest to assess myocardial viability. Dipyridamole was not given to these patients.

Imaging Protocols

For ^{82}Rb scans, subjects received a maximum of 0.02 MBq/kg ^{82}Rb given intravenously with an infusion pump. Dynamic scans were collected for a total of 7 min (thirty-six 5-s frames, eight 15-s frames, and four 30-s frames). For $H_2{}^{15}O$ scans, subjects received a maximum of 0.01 MBq/kg $H_2{}^{15}O$ administered intravenously as a bolus. Dynamic scans were collected for a total of 5 min (twenty-four 5-s frames, six 10-s frames, and eight 15-s frames). After completion of rest scans, subjects received 0.14 mg/kg/min dipyridamole intravenously for 4 min. Four minutes after the end of the dipyridamole infusion, subjects again received ^{82}Rb and $H_2{}^{15}O$. The delay between ^{82}Rb and $H_2{}^{15}O$ after dipyridamole was ~8 min. In subjects receiving $^{13}NH_3$, 0.004–0.007 MBq/kg was administered intravenously over 15 s with a constant infusion pump. The emission scan consisted of 16 frames (10 s × 12, 30 s × 2, 60 s × 1, 900 s × 1) for a total scan time of 19 min. For healthy subjects receiving dipyridamole, 40–60 min later, after radioactivity from $^{13}NH_3$ had returned to background levels, dipyridamole was administered and the imaging sequence was repeated.

Quantification of Myocardial Perfusion in Healthy Volunteers

Emission data were reconstructed and reoriented to short-axis images using a Hann filter with a cutoff frequency of 0.4 cycle/pixel giving a natural resolution of 10 mm (full width at half maximum). The myocardium in each midventricular plane was defined by circumferential analysis and divided into eight ROIs. Time–activity curves derived from ^{82}Rb images were fitted to a previously developed two-compartment model (*6*) to get flow estimates. The fitting process without any wavelet-based maneuver was called the original protocol. The resting and hyperemic estimates for the healthy volunteers were compared with the reference values that were derived from the validated one-compartment model fitting with $H_2{}^{15}O$ data (*3*). Flow estimates from $^{13}NH_3$ were obtained by fitting the dynamic data to a two-compartment model (*17*).

Wavelet-Based Noise Reduction

A discrete dyadic wavelet transform (i.e., with a scaling factor of 2) developed by Laine and Koren (*18–20*) was used for signal analysis and noise reduction in this study. The Fourier transforms of the wavelet function and the scaling function are shown as Equations 1 and 2:

$$\Psi(\omega) = (j\omega)^1(\sin(\omega/4)/(\omega/4))^4 \quad \text{Eq. 1}$$

$$\Phi(\omega) = (\sin(\omega/2)/(\omega/2))^3. \quad \text{Eq. 2}$$

The wavelet analysis used a redundant representation (i.e., down sampling and up sampling were not performed during wavelet expansion and synthesis). This overcomplete representation resulted in shift invariance, avoided aliasing effect, and, therefore, ensured the consistency of noise reduction. The method of thresholding and shrinkage developed by Donoho and Johnstone (*13–15*) and adapted by Lin et al. (*16*) was used to perform noise reduction in this study.

Each midventricular short-axis image of each frame underwent a two-dimensional wavelet denoising process. The wavelet denoising algorithm was applied independently to each short-axis image plane from each frame to remove noise in the spatial domain and then applied independently to each time–activity curve for each ROI to remove noise in the temporal domain. The blood time–activity curve also underwent the denoising process. Time–activity curves from each of eight ROIs from each short-axis plane were analyzed separately. The reconstructed blood and tissue time–activity curves were fitted to appropriate mathematic models (identical to those used for the original protocol) to get flow estimates. Data from healthy volunteers were averaged to provide one mean flow for a heart, but region-to-region variability in flow estimates was also measured. We defined this approach as the wavelet protocol.

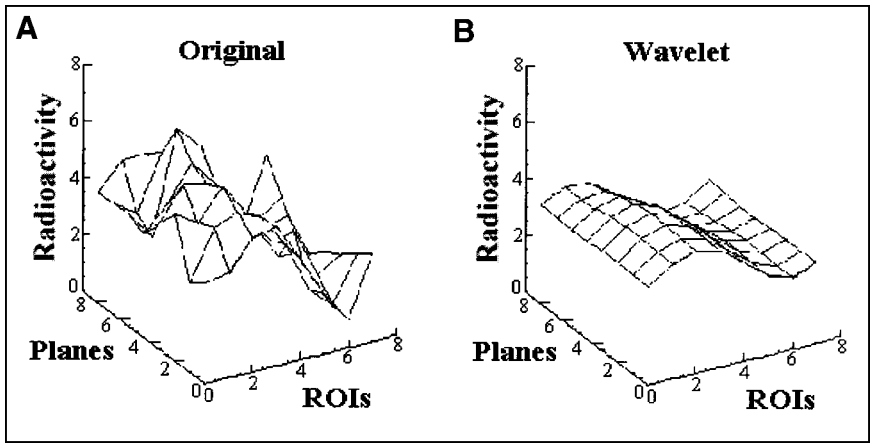

FIGURE 1. Count-based regional radioactivity in last frame of ^{82}Rb scan in patient with myocardial infarction before (A) and after (B) wavelet denoising. *x*-axis represents eight ROIs in each plane (from inferior region 1 counterclockwise to septal), *y*-axis represents average radioactivity (nCi/pixel/s) in ROI, and *z*-axis represents short-axis planes (from base to apex). Regional radioactivity in original dataset for entire heart was distorted by inherent noise (A). Wavelet approach maintained smoothness and continuity among regions but still preserved regional variation (B).

Comparison of Original Protocol and Wavelet Protocol in Healthy Volunteers

The precision of quantification results derived from perfusion images was defined as the ratio of a flow estimate to its associated SE (i.e., the estimate-to-error ratio). The SE resulted from the calculation of the second derivatives of the error function with the values of the optimized estimates. The median of the estimate-to-error ratios of all ROIs was used as an indicator of overall precision for a specific study. Comparison was made between the original protocol and the wavelet protocol at rest and after pharmacologic stress.

The accuracy of the flow estimates obtained from the original protocol and the wavelet protocol using ^{82}Rb images was verified by the reference values obtained from the model fitting with $H_2{}^{15}O$ data. The distribution of differences among the two measurements of all ROIs in all healthy volunteers was found at rest and after pharmacologic stress.

Application of Wavelet Analysis to $H_2{}^{15}O$ and $^{13}NH_3$ Data

In a separate analysis, data derived from $H_2{}^{15}O$ and $^{13}NH_3$ images underwent the same wavelet-denoising process. The denoised data were fitted to their respective models to get flow estimates. The precision in terms of median estimate-to-error ratio was calculated and compared with original estimates.

The coefficients of variation (COVs) (i.e., the ratio of the SD to the average flow in all ROIs) of each healthy subject were used as an indicator of inter-regional heterogeneity. The COV was calculated for each study at rest or after pharmacologic stress.

Comparison of Differentiating Capacity Obtained from Original Protocol with That Derived from Wavelet Protocol in Patients

Myocardial flow was also estimated using dynamic PET with ^{82}Rb in 13 patients undergoing viability scanning. Three experienced nuclear cardiologists were asked to read count-based image sets of ^{82}Rb and FDG scans for the patients. Each ROI in the study was categorized as normal, ischemic but viable, or infarcted. Normal tissue was defined as regions with normal myocardial perfusion and FDG uptake, ischemic regions were defined as those with diminished perfusion but near-normal FDG uptake, and infarcted zones were defined as those with myocardial perfusion $<$ 50% of maximum with a matched decreased in FDG uptake. Differences were resolved by consensus. Flow estimates in the normal regions and infarcted regions were compared without and with the wavelet protocol. The number of ischemic but viable regions in this particular group of patients was too small to be analyzed.

RESULTS

Dynamic Data

Dynamic curves derived from ^{82}Rb images can be viewed through the temporal and the spatial domains. The temporal view shows the shape of time–activity curves over time. The blood and tissue time–activity curves retained the dynamic shapes (including the early peaks), and the inherent noise was removed (*16,19*).

The spatial view represents the radioactivity among all ROIs in the whole heart at a given time. Figure 1 shows regional radioactivity of all ROIs in the last frame (390th to 420th second) of the resting ^{82}Rb scan in one patient with myocardial infarction in the anterior and septal regions. The regional radioactivity derived from raw images was noisy so that the continuity among adjacent regions was not observed. However, the wavelet protocol restored the smoothness of radioactivity in the whole heart and still preserved the regional variation.

Precision and Accuracy

The median estimate-to-noise ratio for myocardial perfusion in all resting ^{82}Rb studies in healthy volunteers (n = 18) was 2.28 $\pm$ 0.65 with the original protocol and 10.70 $\pm$ 3.45 with the wavelet protocol, equivalent to a gain of 4.85 ($P < 0.001$) (Fig. 2). The estimate-to-noise ratio in all hyperemic ^{82}Rb studies (n = 14) was 2.07 $\pm$ 0.68 before and 9.93 $\pm$ 3.69 after the wavelet approach (Fig. 2). The gain was 5.01 ($P < 0.001$).

Flow estimates derived from ^{82}Rb images were compared with those from original $H_2{}^{15}O$ estimates on a region-by-region basis. Results derived from unmodified ^{82}Rb data slightly overestimated flow compared with estimates obtained with $H_2{}^{15}O$ (0.05 $\pm$ 0.80 mL/g/min at rest and 0.53 $\pm$ 1.57 mL/g/min after dipyridamole; n = 560 ROIs at rest compared with 448 ROIs after dipyridamole) and had ex-

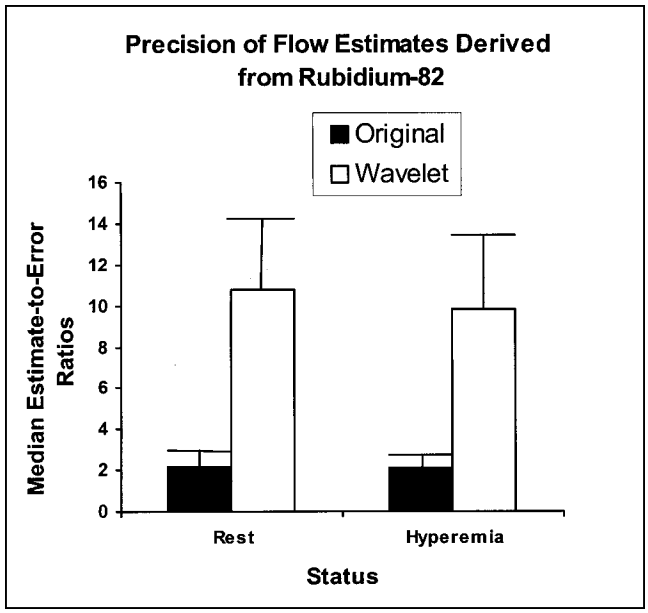

FIGURE 2. Median estimate-to-error ratios derived from ^{82}Rb data before (original) and after wavelet denoising at rest and during hyperemia. Wavelet approach improved estimate-to-noise ratio ($P < 0.001$ for both). Values are expressed as mean ± SD.

tremely wide variation (Fig. 3). The difference in resting flows was −0.09 ± 0.20 mL/g/min and −0.04 ± 0.56 mL/g/min after dipyridamole using the wavelet protocol. Thus, the bias and variation in comparison with $H_2{}^{15}O$ were significantly reduced by wavelet denoising (Fig. 3).

Flow Estimates Derived from $H_2{}^{15}O$ and $^{13}NH_3$

The estimate-to-error ratios of resting flow derived from $H_2{}^{15}O$ data from healthy volunteers was 5.16 ± 0.84 before and 8.70 ± 1.12 after wavelet noise reduction ($P < 0.001$) yielding a gain of 1.72. The precision for hyperemic flow was 4.84 ± 1.37 before and 9.60 ± 2.02 after wavelet denoising ($P < 0.001$) with a gain of 2.25 (Fig. 4A). The COVs of inter-regional flow were reduced from 31% ± 6% to 9% ± 2% at rest ($P < 0.001$) and from 30% ± 6% to 14% ± 5% after hyperemia ($P < 0.001$) using the wavelet approach (Fig. 4B). Thus, the wavelet approach significantly improved the precision of flow estimates and reduced inter-regional heterogeneity.

Flow estimates derived from $^{13}NH_3$ data also showed improved precision and decreased heterogeneity after wavelet processing. Estimate-to-error ratios increased from 4.94 ± 0.61 to 8.95 ± 3.72 at rest ($P < 0.001$) and from 7.70 ± 1.87 to 13.36 ± 4.51 with hyperemia ($P < 0.001$) after wavelet denoising ($n = 7$) (Fig. 5A). The COV decreased from 23% ± 6% to 7% ± 4% at rest ($P < 0.001$) and from 18% ± 4% to 6% ± 1% with hyperemia ($P < 0.001$) after the wavelet process (Fig. 5B).

Flow Estimates in Normal and Infarcted Regions

Flow estimates in the normal and infarcted regions were compared according to the categorization of three specialists. Figure 6 shows the flow distribution in infarcted and normal territories in patients. Because of the poor precision derived from the original protocol, the distributions of flows in the normal and infarcted regions were wide and overlapped with each other. Without the denoising process, the original protocol failed to differentiate regions with normal perfusion from those with low perfusion. The wavelet protocol successfully separated the flow in these two states (Fig. 6). Flow derived from ^{82}Rb after the wavelet protocol was 0.71 ± 0.15 mL/g/min in the normal regions and 0.53 ± 0.14 mL/g/min in infarcted regions ($P < 0.001$). The wavelet approach consistently differentiated normal from infarcted regions in all patients.

DISCUSSION

Although PET is a powerful tool for analyzing various physiologic functions, this study indicates that quantification of myocardial perfusion using uncorrected data derived from ^{82}Rb images cannot produce accurate estimates because dynamic curves are noisy. On the other hand, wavelet analysis and processing provided a robust approach to obtain accurate and precise myocardial flow and to differentiate normal from abnormal regions.

The wavelet-denoising algorithm evaluates local statistics, performs locally adaptive spatial and temporal smooth-

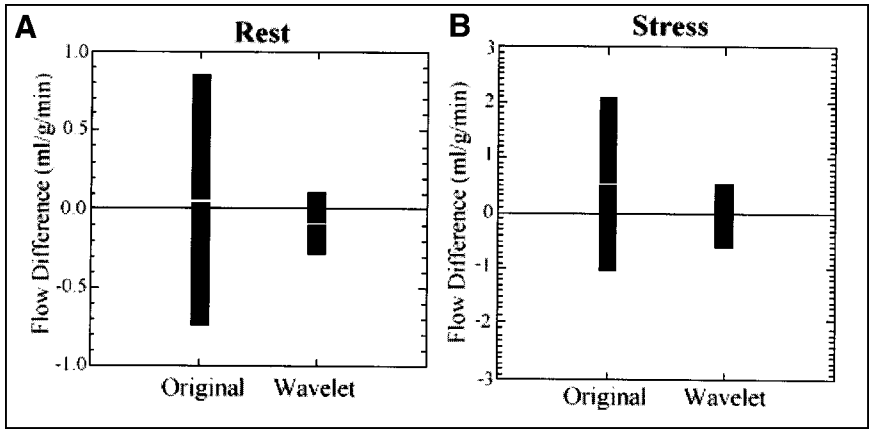

FIGURE 3. Distribution of differences between flows derived from ^{82}Rb studies and those from $H_2{}^{15}O$ studies. (A) Differences in resting flows with original protocol (0.05 ± 0.80 mL/g/min) and wavelet protocol (−0.09 ± 0.20 mL/g/min). (B) Differences in hyperemic flows with original protocol (0.53 ± 1.57 mL/g/min) and wavelet protocol (−0.04 ± 0.56 mL/g/min). Wavelet protocol reduced differences between two measurements ($P < 0.001$ for both). Values are expressed as mean ± SD.

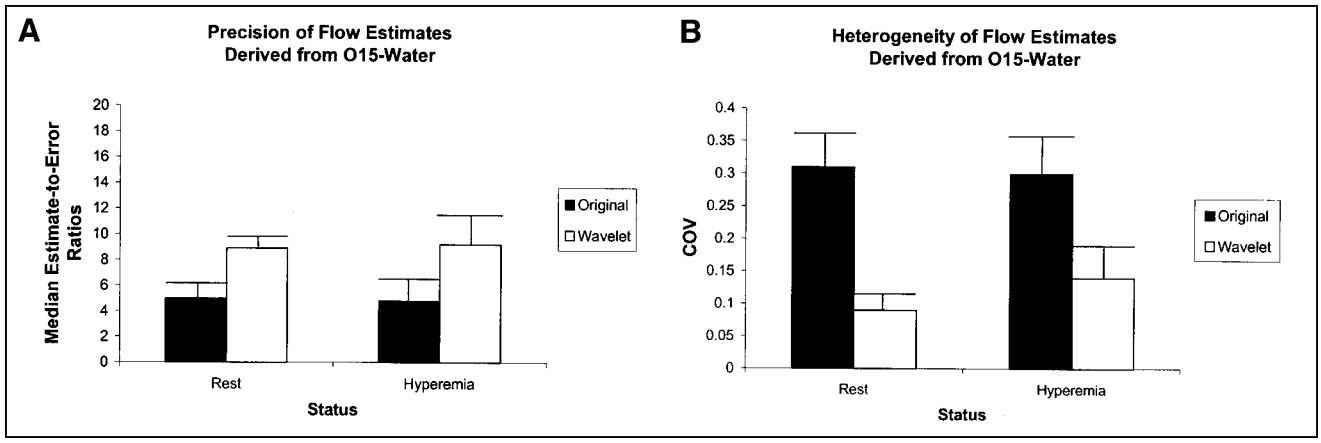

FIGURE 4. Estimate-to-error ratios (A) and COVs of flow estimates (B) derived from $H_2{}^{15}O$ data before and after wavelet-based noise reduction at rest and during hyperemia. Wavelet approach improved precision and reduced regional variation ($P < 0.001$ for both). Values are expressed as mean ± SD.

ing, separates signal and noise, and reconstructs signals that can be fitted to obtain accurate estimates. Wavelet analysis has the ability to adapt to local variation and also has a theoretic proof for finding a near-optimal approximation to an underlying function. This approach can spot and preserve rapid changes in a signal and separate affected and unaffected regions. Therefore, the results in this study show that wavelet transformations and analysis are powerful tools for maintaining the fidelity of multidimensional signals in noise-limited images.

The fidelity of time–activity data improved the quantitative results in several ways. First, the wavelet protocol significantly increased the precision of flow estimates. The estimate-to-error ratio increased about 5-fold in ^{82}Rb studies, whereas the size of ROIs remained the same (~0.70–0.85 cm^3). Therefore, the need to sacrifice the information of detailed textures in return for better statistical stability was eliminated.

Second, the wavelet protocol resulted in regional estimates derived from ^{82}Rb images using the two-compartment model as accurate as those derived from $H_2{}^{15}O$ images using the one-compartment model. Although the wavelet method produced a slight bias (−0.09 mL/g/min) in resting studies, the significant reduction in the variation of difference between the two measurements outperformed the original protocol and ensured the reliability of regional estimates (Fig. 3A). For the stress studies, bias and variation were significantly reduced by wavelet processing (Fig. 3B). The mean bias (−0.04 mL/g/min) can be ignored compared with the relative hyperemia (~2.5–3.5 mL/g/min). Therefore, the wavelet protocol improved the accuracy of regional flow estimates.

Third, this multidimensional wavelet protocol increased the precision and decreased the heterogeneity of flow estimates derived from ^{82}Rb as well as those obtained with $H_2{}^{15}O$ and $^{13}NH_3$. Previous studies from our laboratory (*3*)

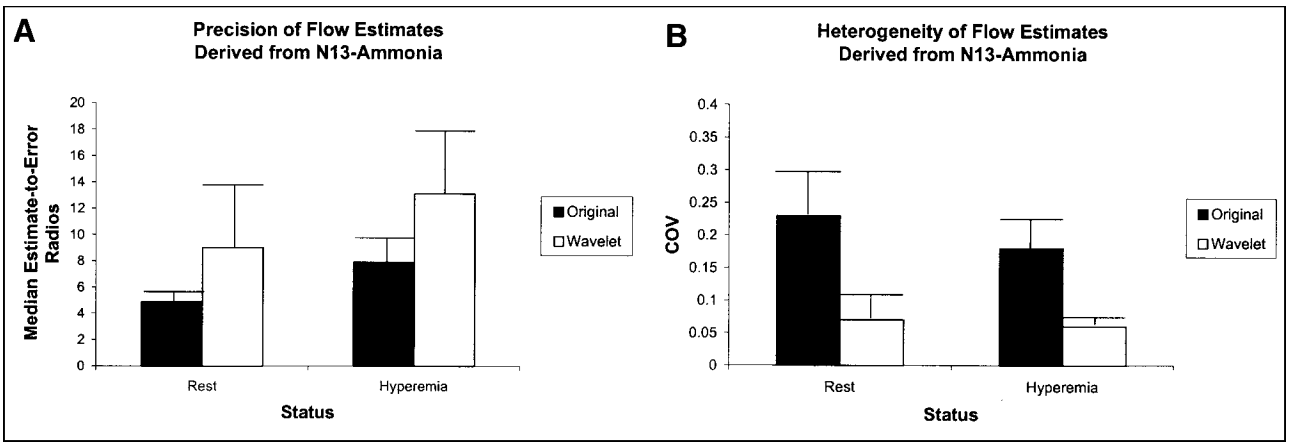

FIGURE 5. Estimate-to-error ratios (A) and COVs of flow estimates (B) derived from $^{13}NH_3$ data before and after wavelet-based noise reduction at rest and during hyperemia. Wavelet approach improved precision and reduced regional variation ($P < 0.001$ for both). Values are expressed as mean ± SD.

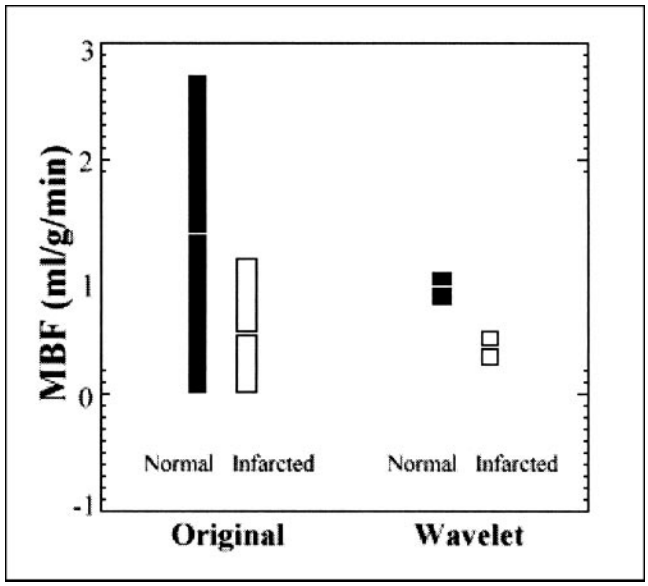

FIGURE 6. Flow estimates in normal and infarcted regions in patients with myocardial infarction using ^{82}Rb at rest. Before wavelet denoising (Original), flow estimates had wide distributions and significant overlap. After wavelet denoising (Wavelet), flow estimates in normal and infarcted regions were clearly separated. Values are expressed as mean ± SD. MBF = myocardial blood flow.

have shown that regional COV in studies from healthy volunteers evaluated with $H_2{}^{15}O$ averages ~20%–35% (*3,20*). This is similar to values that have been observed in experimental studies (*21*). The gain in precision with ^{82}Rb is more significant than that with the other two tracers (five-fold with ^{82}Rb and 2-fold with $H_2{}^{15}O$ and $^{13}NH_3$) because the inherent signal-to-noise ratio is lower in ^{82}Rb images. In addition, wavelet processing did not markedly influence the absolute value of global flows derived from either $H_2{}^{15}O$ or $^{13}NH_3$. However, flow estimates with ^{82}Rb decreased after wavelet denoising because of improved data accuracy (*19*) (Table 1).

Quantitative measurements also proved that flow estimates in the normal and infarcted regions could be discriminated. Therefore, the improvement in the precision and accuracy of flow estimates was not simply associated with oversmoothing. Instead, the wavelet approach exhibits a built-in local adaptivity that detected the transition between normal and infarcted regions. This local adaptivity not only contributed to the differentiating capacity in the spatial domain but also preserved the early upstrokes of blood and time–activity curves (the temporal domain), essential features for getting accurate flow estimates.

Most important, the denoising process followed an objective algorithm that performed wavelet thresholding and shrinkage. Under the assumption of containing a series of normally distributed errors, this algorithm near-optimally separated noise and signal according to the local statistics of wavelet components. The best smoothing effect was mathematically, rather than visually or empirically, determined. Therefore, although PET images from different scans might contain various levels of noise, the described wavelet protocol automatically found an ideal amount to smooth without the need of empiric trial and error. This characteristic enabled the wavelet approach to be generalizable to the evaluation of other parameters in the same compartment model or to quantification using PET with different radioactive tracers.

CONCLUSION

In this study, we showed that the wavelet method successfully improved the precision of flow estimates and reduced the inter-regional heterogeneity in the hearts of healthy volunteers with the use of three different flow tracers. Because of the similarity of the problems and the methods, the use of wavelet-based noise reduction and signal maintenance has significant potential to improve information acquisition from various imaging modalities such as SPECT, CT, and MRI. Therefore, the wavelet method should prove to be a robust approach to improve image quantification and fidelity.

ACKNOWLEDGMENTS

This work was supported in part by grants from the National Heart, Lung, and Blood Institute (grant RO1 HL

TABLE 1
Estimates of Global Flow with Original Protocol and After Wavelet Protocol Processing for Each Flow Tracer in Healthy Volunteers

	Global flow* (mL/g/min)								
	^{82}Rb			$H_2{}^{15}O$			$^{13}NH_3$		
Study	Original	Wavelet	*n*	Original	Wavelet	*n*	Original	Wavelet	*n*
Rest	1.15 ± 0.46	0.82 ± 0.26	18	0.92 ± 0.19	0.90 ± 0.17	18	0.62 ± 0.16	0.59 ± 0.16	7
Stress	2.50 ± 0.54	1.85 ± 0.56	17	1.89 ± 0.50	1.84 ± 0.52	17	1.89 ± 0.67	1.76 ± 0.67	7

*Mean ± SD.

Same subjects received ^{82}Rb and $H_2{}^{15}O$, whereas seven different subjects received $^{13}NH_3$. Mean flow decreased after wavelet protocol with ^{82}Rb because of improved estimates.

46895) and the Jacob and Hilda Blaustein Foundation (grant JB980049).

REFERENCES

1. Schelbert HR, Phelps ME, Huang SC, et al. N-13 ammonia as an indicator of myocardial blood flow. *Circulation*. 1981;63:1259–1272.
2. Bergmann SR, Fox KA, Rand AL, et al. Quantification of regional myocardial blood flow in vivo with $H_2{}^{15}O$. *Circulation*. 1984;70:724–733.
3. Bergmann SR, Herrero P, Markham J, Weinheimer CJ, Walsh MN. Noninvasive quantitation of myocardial blood flow in human subjects with oxygen-15-labeled water and positron emission tomography. *J Am Coll Cardiol*. 1989;14:639–652.
4. Kuhle WG, Porenta G, Huang SC, et al. Quantification of regional myocardial blood flow using ^{13}N-ammonia and reoriented dynamic positron emission tomographic imaging. *Circulation*. 1992;86:1004–1017.
5. Herrero P, Markham J, Shelton ME, Weinheimer CJ, Bergmann SR. Noninvasive quantification of regional myocardial perfusion with rubidium-82 and positron emission tomography: exploration of a mathematical model. *Circulation*. 1990; 82:1377–1386.
6. Herrero P, Markham J, Shelton ME, Bergmann SR. Implementation and evaluation of a two-compartment model for quantification of myocardial perfusion with rubidium-82 and positron emission tomography. *Circ Res*. 1992;70:496–507.
7. Huesman RH. A new fast algorithm for the evaluation of regions of interest and statistical uncertainty in computed tomography. *Phys Med Biol*. 1984;29:543–552.
8. O'Sullivan F. Imaging radiotracer model parameters in PET: a mixture analysis approach. *IEEE Trans Med Imaging*. 1993;12:399–412.
9. O'Sullivan F. Metabolic images from dynamic positron emission tomography studies. *Stat Methods Med Res*. 1994;3:87–101.
10. Huesman RH, Klein GJ, Reutter BW, Coxson PG, Botvinick EH, Budinger TF. Strategies for extraction of quantitative data from volumetric dynamic cardiac positron emission tomography data. *Cardiology*. 1997;88:54–61.
11. Herholz K. Non-stationary spatial filtering and accelerated curve fitting for parametric imaging with dynamic PET. *Eur J Nucl Med*. 1988;14:477–484.
12. Unser M, Aldroubi A. A review of wavelets in biomedical applications. *Proc IEEE*. 1996;84:626–638.
13. Donoho DL, Johnstone IM. Ideal spatial adaptation by wavelet shrinkage. *Biometrika*. 1994;81:425–455.
14. Donoho DL, Johnstone IM. Adapting to unknown smoothness via wavelet shrinkage. *J Am Stat Assoc*. 1995;90:1200–1223.
15. Donoho DL. De-noising by soft-thresholding. *IEEE Trans Inf Theory*. 1995;41: 613–627.
16. Lin JW, Laine A, Bergmann SR. Improving PET-based physiological quantification through wavelet denoising. *IEEE Trans Biomed Eng.* 2001:in press.
17. Choi Y, Huang SC, Hawkins RA, et al. A simplified method for quantification of myocardial blood flow using nitrogen-13-ammonia and dynamic PET. *J Nucl Med*. 1993;34:488–497.
18. Laine A, Koren I. A discrete dyadic wavelet transform for multidimensional feature analysis. In: Akay M, ed. *Time Frequency and Wavelets in Biomedical Signal Processing*. Piscataway, NJ: IEEE; 1998:425–450.
19. Lin J-W, Sciacca RR, Chou R-L, Laine AF, Bergmann SR. Quantification of myocardial perfusion in human subjects using ^{82}Rb and wavelet-based noise reduction. *J Nucl Med.* 2001;42:201–208.
20. Herrero P, Hartman JJ, Senneff MJ, Bergmann SR. Effects of time discrepancies between input and myocardial time-activity curves on estimates of regional myocardial perfusion with PET. *J Nucl Med*. 1994;35:558–566.
21. King RB, Bassingthwaighte JB, Hales JR, Rowell LB. Stability of heterogeneity of myocardial blood flow in normal awake baboons. *Circulation Res.* 1985;57: 285–295.